Progress In Electromagnetics Research M, Vol. 80, 121–131, 2019

Spectral Domain Fast Multipole Method for Solving Integral Equations of Electromagnetic Wave Scattering

Mohammad Ahmad* **and Dayalan Kasilingam**

Abstract—In this paper, a spectral domain implementation of the fast multipole method is presented. It is shown that the aggregation, translation, and disaggregation stages of the fast multipole method (FMM) can be performed using spectral domain (SD) analysis. The spectral domain fast multipole method (SD-FMM) has the advantage of eliminating the near field/far field classification used in conventional FMM formulation. The goal of this study is to investigate the similarities and differences between the spectral domain analysis and conventional FMM formulation. The benefit of the spectral domain analysis such as transforming the convolutional form of the Green's function to a multiplicative form is incorporated in the SD-FMM method. The study focuses on the application of SD-FMM to one-, two-, and three-dimensional electric field integral equation (EFIE). The cases of perfectly electric conducting (PEC) strips, circular perfectly conducting cylinders, and perfectly conductor spheres are analyzed. The results from the SD-FMM method are compared with the results from the conventional FMM and the direct application of Method of Moments (MoM). The SD-FMM results agree well with results from the direct application of MoM.

1. INTRODUCTION

In electromagnetic scattering, many problems can be solved by using boundary-integral methods. For the past several decades, the method of moments (MoM) [1] has been a very popular numerical technique used to solve these integral equations which can be described as linear systems represented by dense matrices. For large scale problems, direct matrix inversion methods are impractical, due to the high computational cost of matrix factorization. In such cases, iterative algorithms are found to be computationally more efficient [2]. Generally, at each iteration step, matrix-vector multiplications cost $O(N^2)$ operations, where N is the number of unknowns in the problem. The corresponding computer memory requirement is $O(N^2)$. In recent years, significant research has been conducted into developing techniques and algorithms to reduce the computational demands of matrix-vector multiplication and associated memory requirements. For surface scatterers such as perfect conductors, the conjugate gradient-fast Fourier transform (CG-FFT) method was shown to enhance the computational performance [3]. It remains as the most efficient fast solver because of its relative simplicity, and it reduces the computational complexity to $O(N \log N)$ operations and memory requirements to $O(N)$. Unfortunately, the necessity of using staircase approximations for geometrical modeling severely restricted its applications [4]. This approximation was later eliminated by the development of pre-corrected fast Fourier transform (PFFT) algorithm (also known as the adaptive integral method (AIM)) which reduces the complexity to $O(N^{3/2} \log N)$ operations and the memory requirements to $O(N^{3/2})$ [5, 6]. These methods use arbitrary basis functions, which are projected on a uniform grid to enable the use of FFT. The Fast Multipole Method proposed by Rokhlin [7, 8] reduces the

Received 16 August 2018, Accepted 1 March 2019, Scheduled 9 April 2019
* Corresponding author: Mohammad Ahmad (mahmad1@umassd.edu).
The authors are with the Department of Electrical and Computer Engineering, University of Massachusetts, Dartmouth, USA.

computational complexity to $O(N^{3/2})$ operations and the required memory to $O(N^{3/2})$. Its recursive, multi-level extension, namely the multi-level fast multipole method (MLFMM), further reduces the complexity of MoM and memory requirements to $O(N \log N)$ [9].

Due to its inherent advantages, the SD approach has been applied to a variety of different computational applications [10–13]. This is because the solution of the problem in the original domain, if at all possible, may be difficult. When transformed into the new domain, the solution of the problem becomes more tractable. In addition, the use of the FFT algorithm in the SD approach makes it very appealing. The goal of this paper is to apply SD-FMM with MoM to solve electromagnetic scattering problems over perfectly conductor surfaces and compare the results with standard MoM and FMM.

2. FORMULATION OF THE PROBLEM

2.1. One- and Two-Dimensional Analyses

2.1.1. Formulation of the Conventional FMM

The zeroth order Hankel function is the Green's function for one- (1D) and two- (2D) dimensional electromagnetic wave scattering [9]. The basic three steps; aggregation, translation, and disaggregation, that is required to be used in the FMM, can be carried out only if we can factorize the Hankel function into a product of three functions: one containing $\rho_q - \rho'_n$, another containing $\rho_p - \rho_q$, and the third one containing $\rho_m - \rho_p$, where ρ_m is the observation point on the scatterer; ρ'_n is any source point on the scatterer; ρ_p is the center of source points belong to the group G_p; and ρ_q is the center of the observation points belonging to another group G_q. Using the addition theorem for the Hankel function [9], one can compute a sum of the Green's functions evaluated at the field point ρ_m due to many source points ρ'_n located in side G_q as [9]

$$\sum_{n=1}^{N} H_0^{(2)}\left(k_0\left|\rho_m - \rho'_n\right|\right) = \frac{1}{2\pi}\int_0^{2\pi} e^{-jk\cdot(\rho_m-\rho_p)}\tilde{\alpha}_{pq}(\alpha)\sum_{n=1}^{N} e^{-jk\cdot(\rho_q-\rho'_n)}d\alpha, \tag{1}$$

where $\tilde{\alpha}_{pq}(\alpha) \approx \sum_{l=-L}^{L} H_l^{(2)}(\beta\rho_{pq})e^{jl(\varphi_{pq}-\alpha-\pi/2)}$ in which φ_{pq} denotes the angle that ρ_{pq} makes with the x-axis, $H_0^{(2)}(\cdot)$ the zeroth order Hankel function of the second kind, $k = k_0(\cos\alpha a_x + \sin\alpha a_y)$, and k_0 the propagation constant. Equation (1) is valid only if $\rho_{pq} > |(\rho_m - \rho_p) + (\rho_q - \rho'_n)|$.

2.1.2. Formulation of the SD-FMM

In SD analysis, the Hankel function can be represented as [14]

$$H_0^{(2)}\left(k_0\left|\rho_m - \rho'_n\right|\right) = \frac{1}{\pi}\int_{-\infty}^{\infty} \frac{e^{-jk_y|y_m-y'_n|}}{k_y} e^{jk_x(x_m-x'_n)}dk_x \tag{2}$$

where $k_y = \sqrt{k_0^2 - k_x^2}$, x'_n, y'_n denote the source coordinates, and x_m, y_m denotes the observation coordinates. Replacing, $x_m = \rho_m\cos\theta$, $x'_n = \rho'_n\cos\theta'$, $y_m = \rho_m\sin\theta$, and $y'_n = \rho'_n\sin\theta'$, Eq. (2) can be written as

$$H_0^{(2)}\left(k_0\left|\rho_m - \rho'_n\right|\right) = \frac{1}{\pi}\int_{-\infty}^{\infty} \frac{e^{-jk_y|\rho_m\sin\theta-\rho'_n\sin\theta'|}}{k_y} e^{jk_x(\rho_m\cos\theta-\rho'_n\cos\theta')}dk_x. \tag{3}$$

Defining $\rho'_n = \rho'_n\cos\theta' a_x + \rho'_n\sin\theta' a_y$, $k^{\mp} = k_x a_x \mp k_y a_y$, and $\rho_m = \rho_m\cos\theta a_x + \rho_m\sin\theta a_y$, Eq. (3) can be written as

$$H_0^{(2)}\left(k_0\left|\rho_m - \rho'_n\right|\right) = \begin{cases} \dfrac{1}{\pi}\displaystyle\int_{-\infty}^{\infty} e^{jk^-\cdot\rho_m}\frac{1}{k_y}e^{-jk^-\cdot\rho'_n}dk_x, & \rho_m\sin\theta > \rho'_n\sin\theta' \\ \dfrac{1}{\pi}\displaystyle\int_{-\infty}^{\infty} e^{jk^+\cdot\rho_m}\frac{1}{k_y}e^{-jk^+\cdot\rho'_n}dk_x, & \rho_m\sin\theta < \rho'_n\sin\theta' \end{cases}. \tag{4}$$

The formulation given in Eq. (4) is what allows one to compute a matrix-vector product using SD-FMM with the advantage of eliminating the near field/far field classification used in conventional FMM formulation. One can now compute a sum of the Green's functions evaluated at the field point ρ_m due to many source points ρ'_n

$$\sum_{n=1}^{N} H_0^{(2)}\left(k_0\left|\rho_m-\rho'_n\right|\right)=\frac{1}{\pi}\int_{-\infty}^{\infty}\frac{e^{jk^{\mp}\cdot\rho_m}}{k_y}\sum_{n=1}^{N}e^{-jk^{\mp}\cdot\rho'_n}dk_x. \tag{5}$$

Equation (5) represents the 1D and 2D SD-FMM where $\sum_{n=1}^{N}\exp(-jk^{\mp}\cdot\rho'_n)$ describes the aggregation component, $1/k_y$ the translation component, and $\exp(jk^{\mp}\cdot\rho_m)$ the disaggregation component. Table 1 shows a comparison between the conventional FMM and SD-FMM. The first point to note is that the integration limits for the FMM are fixed. However, for the SD-FMM the limits are from $-\infty$ to $+\infty$. This kind of integration over improper limits needs to be truncated. Hence, one must replace the $\pm\infty$ to the proper $K_{\max}$ that will lead to the required accuracy. Second, the translation term in the SD-FMM is easier to find and evaluate than FMM. Moreover, the singularity in the translation term in SD-FMM has to be taken care of to get accurate results. Finally, each of the two groups in FMM has a separate translation term. On the other hand, the translation term in SD-FMM is fixed.

Table 1. A comparison between FMM and SD-FMM for 1D and 2D cases.

	FMM	SD-FMM
Integration limits	0 to 2π	$-\infty$ to ∞
Translation	$\sum_{l=-L}^{L} H_l^{(2)}(\beta\rho_{pq})e^{jl(\varphi_{pq}-\alpha-\pi/2)}$	$1/k_y$
Translation	Each 2 groups have their own translator (not constant)	Fixed
Restriction	Valid only if $\rho_{pq}>\lvert(\rho_m-\rho_p)+(\rho_q-\rho'_n)\rvert$	No

2.1.3. The Electric Field Integral Equation for Electromagnetic Scattering from 1D and 2D Perfectly Conductor Surfaces

The solution of electric field integral equation (EFIE) for electromagnetic scattering of TM^z polarized plane waves from 1D and 2D perfectly conductor surfaces in free space using MoM with pulse basis functions and the Dirac delta testing function is given by [15]

$$E_z^{inc}(\rho_m)=\frac{k_0\eta_0}{4}\sum_{n=1}^{N}\alpha_n\int_{w_n}H_0^{(2)}\left(k_0\left|\rho_m-\rho'_n\right|\right)d\rho', \tag{6}$$

where $H_0^{(2)}(\cdot)$ is the zeroth order Hankel function of the second kind, k_0 the propagation constant, η_0 the free space wave impedance of the free space, α_n ithe unknown surface current density on segment n, w_n the size of the nth segment, and $E_z^{inc}(\rho_m)$ the known incident electric fields on the conductor surface, which is given by $E_0\exp(jk(x_m\cos\varphi_i+y_m\sin\varphi_i))$, where E_0 is a constant, and φ_i is the incident angle. Equation (6) will lead to a set of simultaneous equations that can be written in matrix form as

$$E=ZI, \tag{7}$$

where E is a vector filled with the known incident electric field over each segment ($E_z^{inc}(\rho_m)$), I a vector filled with the approximated unknown current density (α_n), and Z the impedance matrix which is filled by [14]

$$Z_{mn}\approx\begin{cases}\dfrac{k_0\eta_0}{4}w_n\left[1-j\dfrac{2}{\pi}\ln\left(\dfrac{1.781k_0w_0}{4\,(2.718)}\right)\right], & m=n\\ \dfrac{k_0\eta_0}{4}w_nH_0^{(2)}\left(k_0\left|\rho_m-\rho'_n\right|\right), & m\neq n\end{cases}. \tag{8}$$

In the conventional FMM, the impedance matrix in Eq. (7) is broken into near and far field components as [4]

$$E = Z_{near} I_{near} + Z_{far} I_{far}. \tag{9}$$

In the SD-FMM approach, the impedance matrix is broken into

$$E = Z^{+} I^{+} + Z^{-} I^{-}. \tag{10}$$

Equation (10) is populated by the terms in Eq. (4), where (+) represents the k^{+} terms and $(-)k^{-}$ terms in Eq. (4). Taking advantage of Eq. (4) to find Eq. (2), the implementation of Eq. (9) is done as follows: (i) first, divide the source points into two groups — one corresponding to k^{+} and the other to k^{-}, (ii) second, the aggregation stage is done by multiplying the unknown current with its source point. For the first observation point, multiply the result from the second step with the translation component, which is fixed for all points and the disaggregation, (iii) third, for the next observation point, adjust the aggregation component that has been found in the previous step to accommodate the new observation point and then multiply it with the translation component and the disaggregation component. Some components which were in the first group may now be in the second group and vice versa. Finally, for each new observation point, keep adjusting the previous aggregation components and then multiplying them with the translation component and the disaggregation.

2.1.4. Dealing with the Singularity and Integration Method

As seen in Eq. (4), the transform of Hankel function has a singularity in the k_y term located at $k = \pm k_x$. This difficulty, though, can be avoided by introducing a small loss in the medium. This may be implemented by assuming that $k = k' - jk''$, where $k'' \to 0^{+}$. In addition, a change of variable around the singularity has been made, where $k_x = k\cos(t)$. The integration has been done using the Clenshaw-Curtis quadrature method [16] and the $\pm$ infinity limits of integration replaced by $\pm K_{\max}$.

2.2. Three-Dimensional Analyses

2.2.1. Formulation of the Conventional FMM

Similar to 1D and 2D cases, the basic three steps, in FMM, can be carried out only if one can factorize the Green's function into a product of three functions: one containing $r_q - r'$, another containing $r_p - r_q$, and the third one containing $r - r_p$, where r is the observation point on the scatterer; r' is any source point on the scatterer; r_p is the center of source points belong to the group G_p; and r_q is the center of the observation points belong to another group G_q. Using the addition theorem for the three-dimensional (3D) Green's function to compute the sum of the Green's functions evaluated at the field point r_m due to many source points r'_n located inside group G_q as [9]

$$\sum_{n=1}^{N} \frac{\exp(-jk_0|r_m - r'_n|)}{|r_m - r'_n|} = \frac{-jk_0}{4\pi} \int_0^{2\pi} \int_0^{\pi} e^{(-jk\cdot(r_m - r_p))} T_L(k \cdot r_{pq}) \sum_{n=1}^{N} e^{(-jk\cdot(r_q - r'_n))} \sin(\alpha) d\alpha d\beta, \tag{11}$$

where $T_l(k \cdot r_{pq}) = \sum_{l=0}^{L} (-j)^l (2l+1) h_1^{(2)}(k_0 r_{pq}) P_l(k \cdot r_{pq})$, $P_l(x)$ is the Legendre polynomial of order l, $h_1^{(2)}(x)$ is the spherical Hankel function of the second kind. The integral is performed over a unit sphere and $k = k_0(\cos(\beta)\sin(\alpha)a_x + \sin(\beta)\sin(\alpha)a_y + \cos(\alpha)a_z)$. Equation (11) is valid only if $r_{pq} > |(r - r_p) + (r_q - r')|$.

2.2.2. Formulation of the SD-FMM

As seen in Eq. (11), the Green's function for 3D electromagnetic wave scattering is given by

$$G(r, r') = \frac{e^{-jk_0|r - r'|}}{4\pi|r - r'|}. \tag{12}$$

In SD analysis, the Green's function for 3D case can be represented as [14]

$$\frac{e^{-jk_0|r-r'|}}{|r-r'|} = \frac{-j}{2\pi}\int_{-\infty}^{\infty}\int_{-\infty}^{\infty}\frac{e^{-jk_z|z-z'|}}{k_z}e^{j(k_x(x-x')+k_y(y-y'))}dk_xdk_y, \tag{13}$$

where $k_x,\ k_y,\ k_z$ are the Fourier or spectral variables with $k_z = \sqrt{k_0^2-(k_x^2+k_y^2)}$, and x', y', z' and x, y, z denote the source and observation coordinates, respectively. Rewriting Eq. (13) in polar coordinate in terms of (ρ, ψ) by substituting $k_x = \rho\cos\psi$, $k_y = \rho\sin\psi$, and $\rho^2 = k_x^2 + k_y^2$, one gets

$$\frac{e^{-jk_0|r-r'|}}{|r-r'|} = \frac{-j}{2\pi}\int_{0}^{\infty}\int_{0}^{2\pi}\frac{e^{-jk_\rho|z-z'|}}{k_\rho}e^{j(\rho\cos\psi(x-x')+\rho\sin\psi(y-y'))}\rho d\psi d\rho, \tag{14}$$

where $k_\rho = \sqrt{k_0^2-\rho^2}$. Separating the source point from the observation point in Eq. (14) and taking into account the absolute value term, $|z-z'|$, yields

$$\frac{e^{-jk|r-r'|}}{|r-r'|} = \frac{-j}{2\pi}\int_{0}^{\infty}\int_{0}^{2\pi}e^{j(\mp k_\rho z+\rho\cos\psi x+\rho\sin\psi y)}\frac{1}{k_\rho}e^{-j(\mp k_\rho z'+\rho\cos\psi x'+\rho\sin\psi y')}\rho d\psi d\rho. \tag{15}$$

In the $\mp k_\rho$ term, the negative sign will be used if $z > z'$, and the positive sign will be used if $z < z'$. One can now compute a sum of Green's functions evaluated at the observation point r_m due to many source points r'_n as

$$\sum_{n=1}^{N}\frac{e^{-jk_0|r_m-r'_n|}}{|r_m-r'_n|} = \frac{-j}{2\pi}\int_{0}^{\infty}\int_{0}^{2\pi}e^{j(\mp k_\rho z_m+\rho\cos\psi x_m+\rho\sin\psi y_m)}\frac{1}{k_\rho}\sum_{n=1}^{N}e^{-j(\mp k_\rho z'_n+\rho\cos\psi x'_n+\rho\sin\psi y'_n)}\rho d\psi d\rho. \tag{16}$$

The arrangement in Eq. (16) allows one to compute a matrix-vector product with advantage of eliminating the near field/far field classification used in conventional FMM formulation. Equation (16) represents the 3D SD-FMM where $\sum_{n=1}^{N}\exp(-j(\mp k_\rho z'_n + \rho\cos\psi x'_n + \rho\sin\psi y'_n))$ describes the aggregation component; $1/k_\rho$ describes the translation component; and $\exp(j(\mp k_\rho z_m + \rho\cos\psi x_m + \rho\sin\psi y_m))$ describes the disaggregation component. Table 2 shows a comparison between the conventional FMM and SD-FMM in 3D case. One notes from Table 2 that the same points that have been identified in Table 1 are observed here.

Table 2. A comparison between FMM and SD-FMM for 3D case.

	FMM	SD-FMM
Integration limits	0 to π 0 to 2π	$-\infty$ to ∞ $-\infty$ to ∞
Translation	$\sum_{l=0}^{L}(-j)^l(2l+1)h_1^{(2)}(k_0r)P_l(\hat{k}\cdot\hat{r}_{pq})$	$1/k_\rho$
Translation	Each 2 groups have their own translator (not constant)	fixed
Restriction	Valid only if $r_{pq} > \|(r-r_p)+(r_q-r')\|$	No

2.2.3. The EFIE for Electromagnetic Scattering from 3D Perfectly Conducting Surfaces

The matrix form of N^2 system of linear equations that are obtained by applying EFIE for electromagnetic scattering of TM^z polarized plane waves from 3D perfectly conductor shapes in free space using MoM with RWG basis function is given by [17]

$$E = ZI, \tag{17}$$

where $Z = [Z_{mn}]$ is an N^2 matrix, and $I = [I_n]$ and $E = [E_m]$ are column vectors of length N. Elements of Z and E are given by

$$Z_{mn} = l_m \left[j\omega \left(A^+_{mn} \cdot \frac{\rho^{c+}_m}{2} + A^-_{mn} \cdot \frac{\rho^{c-}_m}{2} \right) + \Phi^-_{mn} - \Phi^+_{mn} \right] \tag{18}$$

$$V_m = l_m \left(E^+_m \cdot \frac{\rho^{c+}_m}{2} + E^-_m \cdot \frac{\rho^{c-}_m}{2} \right), \tag{19}$$

where

$$A^\pm_{mn} = \frac{\mu}{4\pi} \int\limits_S f_n(r') \frac{e^{-jkR^\pm_m}}{R^\pm_m} dS', \tag{20}$$

$$\Phi^\pm_{mn} = -\frac{1}{4\pi j\omega\varepsilon} \int\limits_S \nabla_s{}' \cdot f_n(r') \frac{e^{-jkR^\pm_m}}{R^\pm_m} dS' \tag{21}$$

where

$$f_n(r) = \begin{cases} \dfrac{l_n}{2A^+_n} \rho^+_n(r) & \text{if} \quad r \in T^+_n \\ \dfrac{l_n}{2A^-_n} \rho^-_n(r) & \text{if} \quad r \in T^-_n \end{cases} \tag{22}$$

where $\rho^+_n(r)$ is the vector from the vertex of T^+_n opposite to l_n and r; $\rho^-_n(r)$ is the vector from r to the vertex of T^-_n opposite to l_n; $A^\pm_n$ is the area of the triangle $T^\pm_n$, and

$$E^i(r) = \left(E_\theta \hat{\theta}_0 + E_\varphi \hat{\varphi}_0 \right) e^{jk \cdot r} \tag{23}$$

where the propagation vector k is

$$k = k \left(\sin\theta_0 \cos\varphi_0 \hat{x} + \sin\theta_0 \sin\varphi_0 \hat{y} + \cos\theta_0 \hat{z} \right) \tag{24}$$

where $(\hat{\theta}_0, \hat{\varphi}_0)$ defines the angle of arrival of the plane wave in terms of the usual spherical coordinate convention. Unit vectors $\hat{\theta}_0$ and $\hat{\varphi}_0$ are constant vectors which coincide with the usual spherical coordinate unit vectors at points on the line from the origin in the direction of k.

3. RESULTS AND DISCUSSION

This section presents numerical results for the validation of the SD-FMM method by comparing the results obtained from the left side of Eq. (5) with that from the right side of the same equation for 1D and 2D cases, and the left side of Eq. (11) with the right side of the same equation for 3D case. Also, the SD-FMM method is validated by solving canonical 1D, 2D, and 3D scattering problems and comparing these results with results from MoM and FMM.

Table 3 shows the comparison for the 1D case. The source and receiver points are assumed to be distributed over 1D axis for different lengths. To assess how the SD-FMM approach will work with MoM, the root mean square error (RMSE) between the left hand side and right hand side of Eq. (5) is calculated for all observation points, and the average of total RMSE (ARMSE) is computed for this error. The number of the observation and source points is 64 for all sizes. The original integral has integration limits truncated at $K_{\max}$. The results demonstrate excellent accuracy for the selected $K_{\max}$.

Table 3. The ARMSE for the 1D case for different lengths and the appropriate $K_{\max}$.

Length	2λ	5λ	10λ	15λ
ARMSE $\times 10^{-6}$	2.6285	4.7716	7.6989	9.7772
$K_{\max}$	15079	15079	3216	2412

Also, the initial results show that SD-FMM can be performed on different sizes without sacrificing accuracy. Moreover, one notes that as the source and observation points are distributed over wider strips, the truncation limit, $K_{\max}$, is reduced significantly.

Table 4 shows the comparison for 2D case. The source and observation points are assumed to be distributed on circular cylinders with different radii. The same procedure used for 1D case is repeated for 2D case. The number of the receiver and source points is 33 for all sizes. The results demonstrate excellent accuracy for all tested radii with appropriate $K_{\max}$. Also, one notes that as the radius gets larger, $K_{\max}$ is reduced significantly.

Table 4. The ARMSE for the 2D case for different radii and the appropriate $K_{\max}$.

Radius	λ	5λ	10λ	15λ
ARMSE $\times 10^{-6}$	3.9612	5.7342	8.7680	9.2467
$K_{\max}$	700	100	70	45

Table 5 shows the comparison for the 3D case. The source and observation points are assumed to be distributed over a sphere with different radii. The same procedure used for 1D case is used for the 3D case. The number of the receiver and source points is 44 for all sizes. The results demonstrate good accuracy for all tested radii with appropriate $K_{\max}$. Also, one notes that as the sphere gets larger, the value of $K_{\max}$ is reduced significantly.

The first example of electromagnetic wave scattering is from a conducting strip. Fig. 1 shows the induced current density that has been found using 1D SD-FMM and compared for accuracy with MoM

Table 5. The average RMSE for the 3D case for different radii and the appropriate $K_{\max}$.

Radius	λ	5λ	10λ	15λ
ARMSE	4.3174×10^{-5}	4.4129×10^{-6}	4.5252×10^{-6}	6.8937×10^{-6}
$K_{\max}$	725	161	80	53

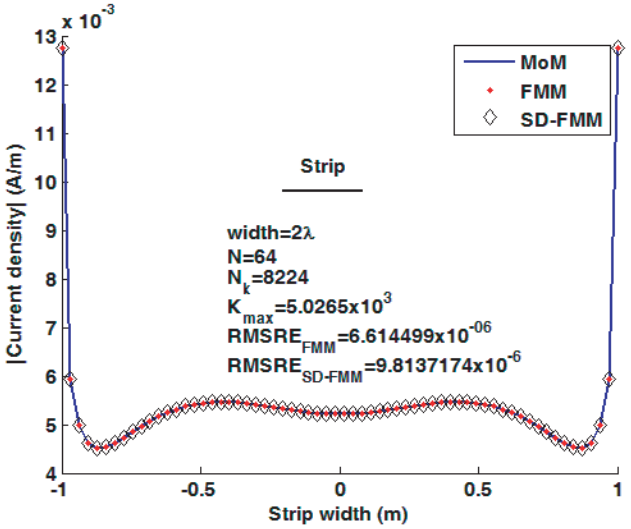

Figure 1. The induced current density on a conducting strip generated using SD-FMM and the MoM.

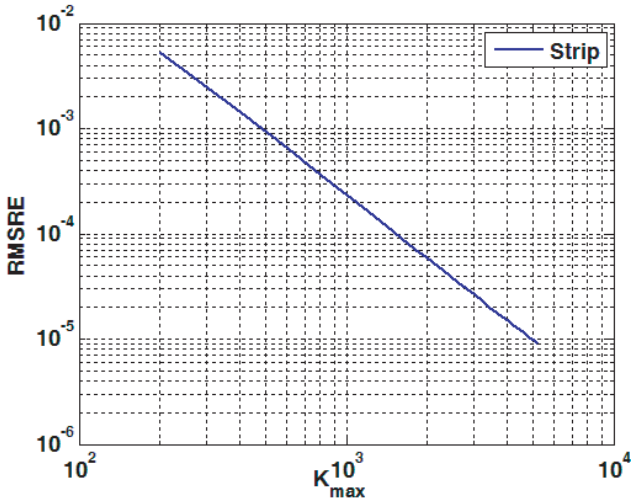

Figure 2. RMSRE versus $K_{\max}$ for the conducting strip problem.

and FMM. The results clearly indicate that the results produced by the proposed SD-FMM method agree well with the MoM and FMM. Fig. 2 and Fig. 3 show the RMS relative error (RMSRE) for the previous example as a function of $K_{\max}$ and N_k, respectively, for the proposed SD-FMM where N_k is the number of points required to perform the integration in Eq. (5). Fig. 4 shows the comparison of the speed among the three methods.

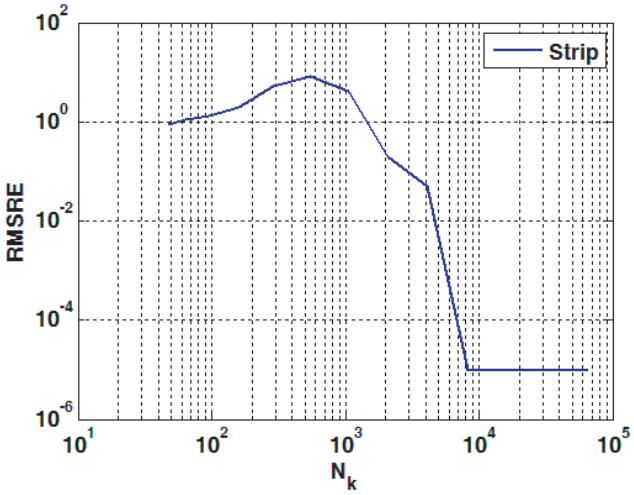

Figure 3. RMSRE versus N_k for the conducting strip problem.

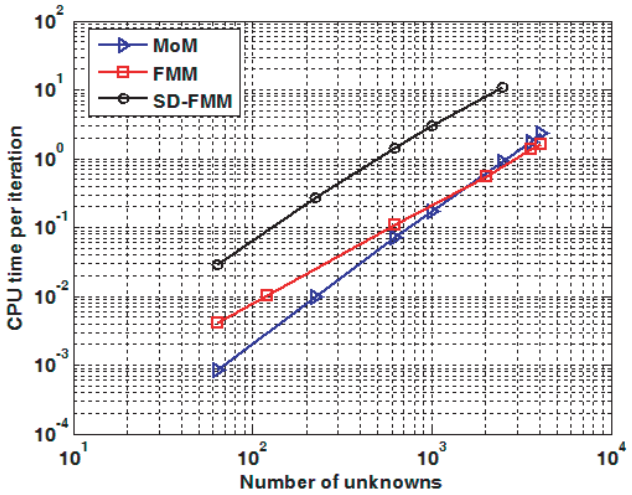

Figure 4. CPU time per iteration for the conducting strip.

For scattering from 2D objects, SD-FMM method is applied to electromagnetic wave scattering from circular, perfectly conducting cylinders. The induced current for circular perfectly conducting cylinder is shown in Fig. 5. A TM^z plane wave is assumed to be incident at $\varphi = 0°$. Fig. 6 and Fig. 7 show the RMSRE for the previous example as a function of $K_{\max}$ and N_k, respectively, for the proposed SD-FMM. Fig. 8 shows the comparison of the speed among the three methods. Table 6 shows the number of operations and memory requirements for both FMM and SD-FMM for 1D and 2D cases.

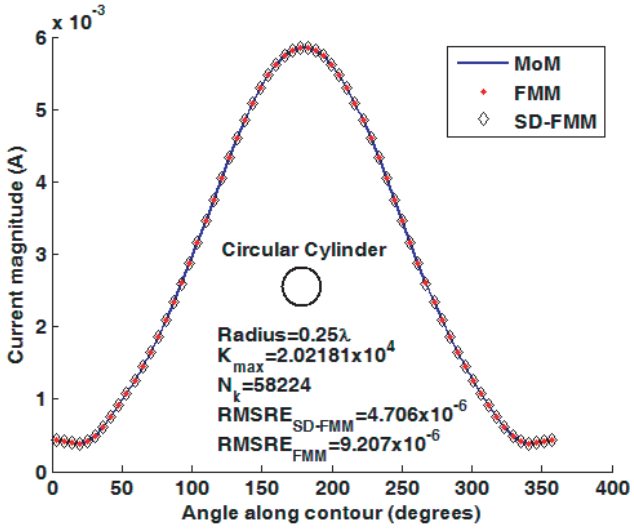

Figure 5. The induced current on a circular cylinder generated by the proposed SD-FMM and the MoM.

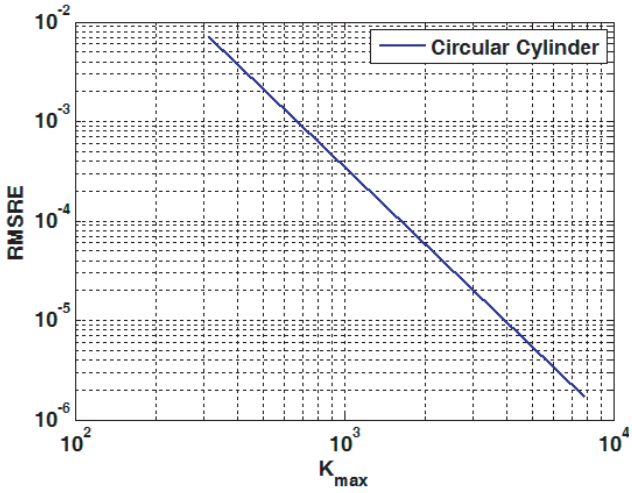

Figure 6. RMSRE versus $K_{\max}$ for the circular cylinder problem.

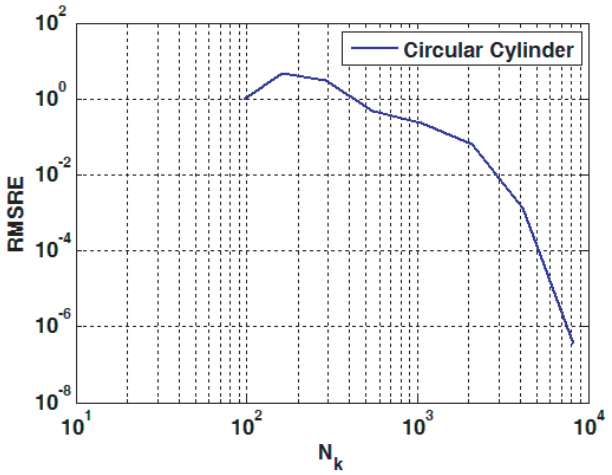

Figure 7. RMSRE versus N_k for circular cylinder.

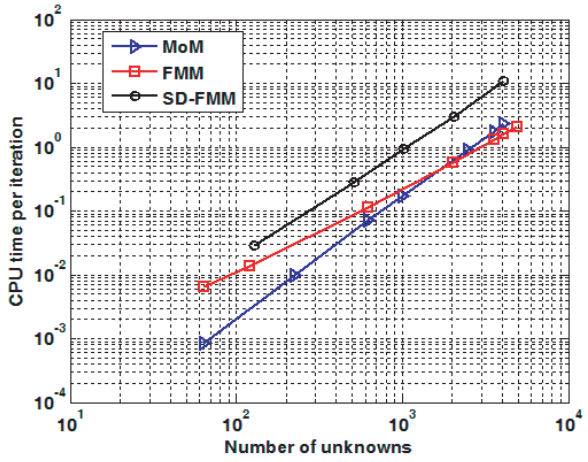

Figure 8. CPU time per iteration for the circular cylinder.

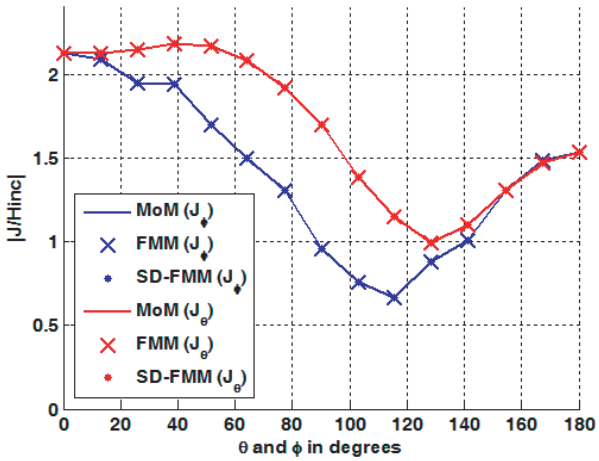

Figure 9. Distribution of current on a 0.2λ radius conducting sphere.

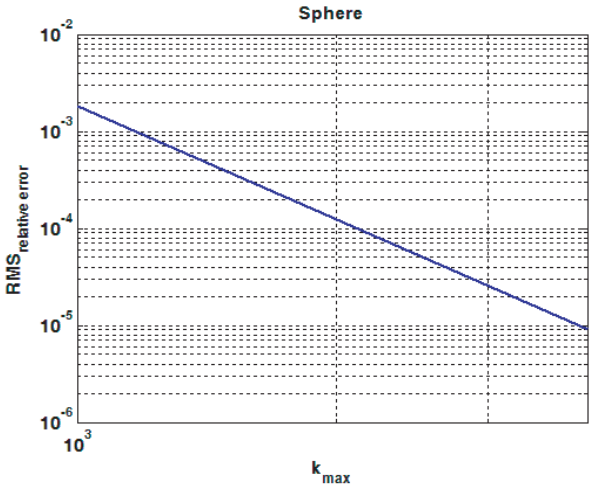

Figure 10. RMSRE versus $K_{\max}$ for the PEC sphere.

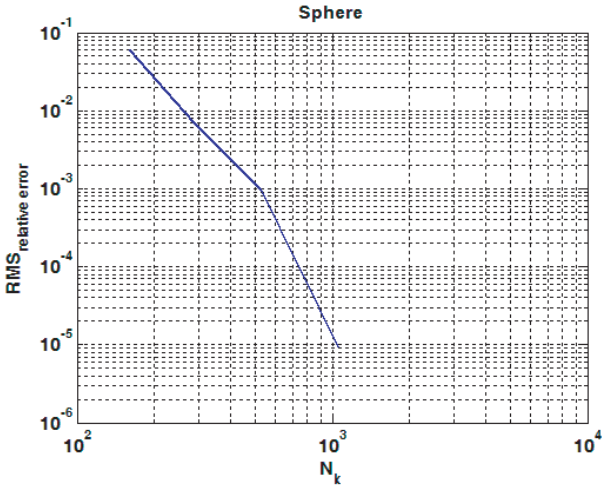

Figure 11. RMSRE versus N_k for the PEC sphere problem.

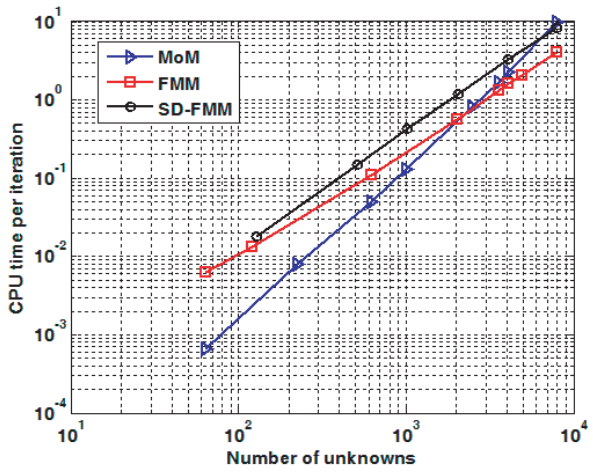

Figure 12. CPU time per iteration for the PEC sphere problem.

Table 6. Numerical comparison between the FMM and the SD-FMM: number of operations.

N: is the number of total basis functions. M: is the number basis functions in each group. R: number of points required in α-domain for the FMM integral. N_k: number of points required in k-domain for the SD-FMM integral.	Number of operations and memory require FMM	Number of operations and memory require SD-FMM
Near-field interactions	$3\ (M \times M) \times (N/M) = 3MN$	0
Aggregation	$R \times N$	$N_k \times N$
Translation	$R \times (N/M)^2$	0
Disaggregation	$R \times N$	$N_k \times N$
Total number of operations = (sum of all operation in column)	$3RN + 3N^{3/2}$ (when $M = N^{1/2}$)	$2N_k \times N$
Total number of operations for $N_k = 128N$ to get an error 10^{-6} and $R = M = N^{1/2}$ and to an error 10^{-6}	$6N^{3/2}$ (faster)	$256N^2$

Figure 9 shows the computed current distribution along the principal cuts through a PEC sphere with a radius of 0.2λ using SD-FMM. The incident field is assumed to be from the negative x-direction. The plane wave has only one component in the z-direction, $E_z = 1$. The cases of axial and equatorial incidence are both considered. The number of triangles used to represent the sphere is 1244. The RMSRE for FMM and SD-FMM are 4.3278×10^{-6} and 9.0338×10^{-6}, respectively. The selection of the limit of the integral and the number of points required to perform the integration were $K_{\max} = 4000$ and $N_k = 1032$, respectively. Fig. 10 and Fig. 11 show the RMSRE versus $K_{\max}$ and N_k, respectively. Fig. 12 shows the time required to do the multiplication between the impedance matrix and the unknown basis functions. Table 7 shows the comparison of the number of operations between FMM and SD-FMM for the 3D case.

Table 7. Numerical comparison between the FMM and the SD-FMM: number of operations and memory requires for 3D case.

N: is the number of total basis functions, M: is the number basis functions in each group, (N/M): is the number of groups in the problem, B: all nearby groups including itself, K: is the number of points that is required to do the integration $K = 2L^2$, where L is the number of points for integration from 0 to pi.	Number of operations and memory for FMM	Number of operations and memory SD-FMM
Near-field interactions	$B(M \times M) \times (N/M) = BMN$	0
Aggregation	$K \times M \times (N/M) = K \times N$	$N_k \times N$
Translation	$K \times (N/M)^2$	0
Disaggregation	$K \times N$	$N_k \times N$
Total number of operations =	$BMN + KN + K \times (N/M)^2 + KN$	$2N_kN$
Total number of operations when $M = L^2$ and $(N/M) = N^{1/2}$. $N_k = 0.25N$	$N^{3/2}$	$0.5N^2$

4. CONCLUSIONS

In this paper, it has been shown that the aggregation, translation, and disaggregation stages of the FMM can be performed using SD analysis. Also, the analytical comparison between the SD-FMM and conventional FMM shows that the SD-FMM code is easier to build and eliminates the near field/far field classification used in conventional FMM formulation. In addition, the new approach gives excellent accuracy compared with the MoM solution for 1D, 2D, and 3D cases. The SD-FMM approach is applied to solving electromagnetic wave scattering from 1D, 2D, and 3D perfectly conductor surfaces. Numerical results from the analysis of scattering from conducting strips, circular cylinders, and spheres have been presented. The numerical results indicate that the proposed method can estimate the induced current densities with comparable accuracy as the conventional FMM and MoM.

REFERENCES

1. Harrington, R. F., *Field Computation by Moment Method*, R. E. Krieger Publ. Com., FL, 1968.
2. Saad, Y., *Iterative Methods for Sparse Linear Systems*, 1st Edition, PWS, 1996.
3. Sarkar, T. K., E. Arvas, and S. M. Rao, "Application of FFT and the conjugate gradient method for the solution of electromagnetic radiation from electrically large and small conducting bodies," *IEEE Trans. Antennas Propagat.*, Vol. 34, No. 5, 635–640, 1986.
4. Jin, J., *Theory and Computation of Electromagnetic Fields*, John Wiley & Sons, 2010.
5. Bleszynski, E., M. Bleszynski, and T. Jaroszewicz, "A fast integral-equation solver for electromagnetic scattering problems," *IEEE AP-S Int. Antennas Propag. Symp. Dig.*, Vol. 1, 416–419, Seattle, WA, USA, Jun. 20–24, 1994.
6. Bleszynski, E., M. Bleszynski, and T. Jaroszewicz, "AIM: Adaptive integral method for solving large-scale electromagnetic scattering and radiation problems," *Radio Sci.*, Vol. 31, No. 5, 1225–1251, Sep.–Oct. 1996.
7. Rokhlin, V., "Rapid solutions of integral equations of scattering theory in two dimensions," *J. Comput. Phys.*, Vol. 86, No. 2, 414–439, Feb. 1990.
8. Coifman, R., V. Rokhlin, and S. Wandzura, "The fast multipole method for the wave equation: A pedestrian prescription," *IEEE Antennas Prop. Mag.*, Vol. 35, No. 3, 7–12, Jun. 1993.
9. Chew, W. C., J. M. Jin, E. Michielssen, and J. Song, *Fast and Efficient Algorithms in Computational Electromagnetics*, Artech House, Norwood, MA, 2001.
10. Moharam, M. G. and T. K. Gaylord, "Rigorous coupled-wave analysis of planar-grating diffraction," *Journal of the Optical Society of America*, Vol. 73, No. 4, 811–818, 1981.
11. Chandezon, J., D. Maystre, and G. Raoult, "A new theoretical method for diffraction gratings and its numerical application," *Journal of Optics*, Vol. 11, No. 4, 235–241, 1980.
12. Van Beurden, M. C., "Fast convergence with spectral volume integral equation for crossed block-shaped gratings with improved material interface conditions," *Journal of the Optical Society of America A*, Vol. 28, No. 11, 226–2278, 2011.
13. Dilz, R. J. and M. C. van Beurden, "An efficient complex spectral path formulation for simulating the 2D TE scattering problem in a layered medium using Gabor frames," *Journal of Computational Physics*, Vol. 345, 528–542, 2017.
14. Volakis, J. and K. Sertel, *Integral Equation Methods for Electromagnetics*, SciTech Publishing, 2012.
15. Grag, R., *Analytical and Computational Methods in Electromagnetics*, Artech House, MA, 2008.
16. Kythe, K. and M. R. Schaferkotter, *Handbook of Computational Methods for Integration*, CRC Press, 2005.
17. Rao, S. M., D. R. Wilton, and A. W. Glisson, "Electromagnetic scattering by surfaces of arbitrary shape," *IEEE Trans. Antennas Propagat.*, Vol. 30, No. 3, 409–418, May 1982.